Volume 9 | Number 43 | 21 November 2017 | Pages 16489–17148

Nanoscale

rsc.li/nanoscale

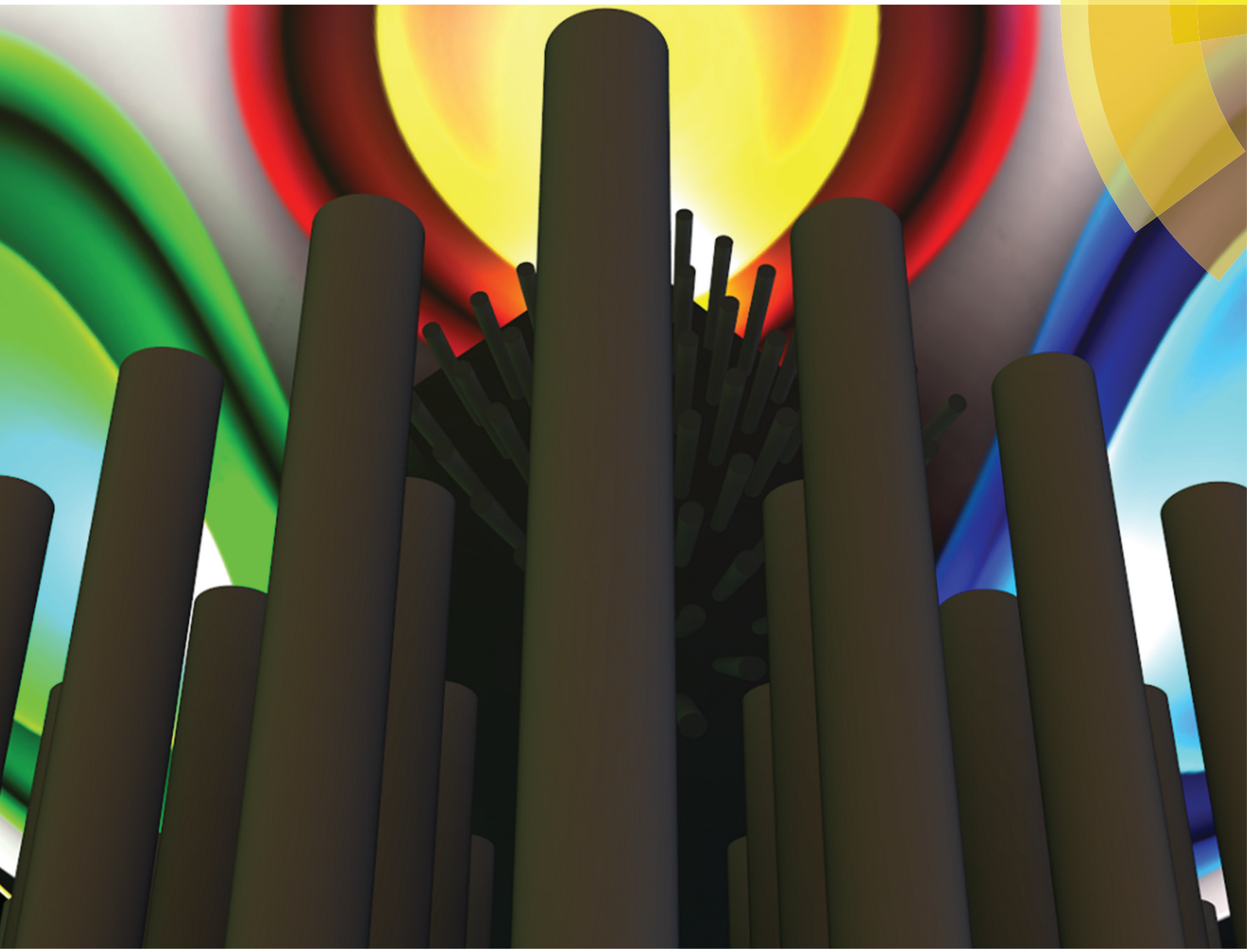

ISSN 2040-3372

ROYAL SOCIETY OF CHEMISTRY

PAPER

Amir Ghobadi, Ekmel Ozbay *et al.*

97 percent light absorption in an ultrabroadband frequency range utilizing an ultrathin metal layer: randomly oriented, densely packed dielectric nanowires as an excellent light trapping scaffold

NCNST

Nanoscale

PAPER

View Article Online
View Journal | View Issue

Cite this: *Nanoscale*, 2017, **9**, 16652

97 percent light absorption in an ultrabroadband frequency range utilizing an ultrathin metal layer: randomly oriented, densely packed dielectric nanowires as an excellent light trapping scaffold†

Amir Ghobadi, *[a,b] Sina Abedini Dereshgi,[a,b] Hodjat Hajian,[a] Gizem Birant,[c,d] Bayram Butun,[a] Alpan Bek[c,d,e] and Ekmel Ozbay*[a,b,f,g]

In this paper, we propose a facile and large scale compatible design to obtain perfect ultrabroadband light absorption using metal-dielectric core–shell nanowires. The design consists of atomic layer deposited (ALD) Pt metal uniformly wrapped around hydrothermally grown titanium dioxide (TiO_2) nanowires. It is found that the randomly oriented dense TiO_2 nanowires can impose excellent light trapping properties where the existence of an ultrathin Pt layer (with a thickness of 10 nm) can absorb the light in an ultra-broadband frequency range with an amount near unity. Throughout this study, we first investigate the formation of resonant modes in the metallic nanowires. Our findings prove that a nanowire structure can support multiple longitudinal localized surface plasmons (LSPs) along its axis together with transverse resonance modes. Our investigations showed that the spectral position of these resonance peaks can be tuned with the length, radius, and orientation of the nanowire. Therefore, TiO_2 random nanowires can contain all of these features simultaneously in which the superposition of responses for these different geometries leads to a flat perfect light absorption. The obtained results demonstrate that taking unique advantages of the ALD method, together with excellent light trapping of chemically synthesized nanowires, a perfect, bifacial, wide angle, and large scale compatible absorber can be made where an excellent performance is achieved while using less materials.

Received 12th June 2017,
Accepted 21st August 2017

DOI: 10.1039/c7nr04186a

rsc.li/nanoscale

Introduction

Electromagnetic (EM) light absorption utilizing subwavelength geometries has been the subject of several studies in the field of nanophotonics and nanoplasmonics. A variety of applications including sensing[1–4] and spectroscopy,[5,6] photovoltaic and thermal photovoltaic,[7,8] and photodetection[9] are examples of these research studies. In 2008, it was experimentally demonstrated that a low density carbon nanotube (CNT) array can act as an extreme dark material.[10] However, in addition to their bulky sparse and fragile feature, material-based absorbers have essentially inherent absorption properties and their response cannot be extended toward longer wavelengths. From there on, several studies were conducted to find a functional architecture to achieve an ultra-broadband absorption response in a thinner design. Owing to their extraordinary EM response and subwavelength geometry, metamaterials and plasmonic designs have attracted extensive attention to realize perfect ultra-broadband light absorption.

Landy *et al.* proposed a single wavelength perfect absorber based on a metallic split ring resonator.[11] Other metamaterial-based architectures were later employed to improve the absorption response of the design.[12–15] However, due to the lack of trapping and confinement mechanisms, this ultrathin single plasmonic layer has inherently a low absorption limit and it can absorb just a fraction of the light. This restriction was later mitigated by introducing a metallic back reflecting layer where this layer acts as an ideal mirror which reflects the whole light spectrum.[16,17] In this configuration, a metal–insulator–metal (MIM) cavity is utilized to trap light inside the design and

[a]*NANOTAM-Nanotechnology Research Center, Bilkent University, 06800 Ankara, Turkey. E-mail: amir@ee.bilkent.edu.tr, ozbay@bilkent.edu.tr*
[b]*Department of Electrical and Electronics Engineering, Bilkent University, 06800 Ankara, Turkey*
[c]*Center for Solar Energy Research and Applications (GUNAM), Middle East Technical University, Ankara 06800, Turkey*
[d]*Micro and Nanotechnology Program, Middle East Technical University, Ankara 06800, Turkey*
[e]*Department of Physics, Middle East Technical University, Ankara 06800, Turkey*
[f]*Department of Physics, Bilkent University, 06800 Ankara, Turkey*
[g]*UNAM-Institute of Materials Science and Nanotechnology, Bilkent University, Ankara, Turkey*

†Electronic supplementary information (ESI) available. See DOI: 10.1039/c7nr04186a

consequently absorption near unity can be achieved. However, all of the aforementioned designs have a narrowband frequency response which restricts their functionality. In general, in an MIM cavity-based absorber, which works based on reflected/transmitted light cancellation, near zero reflection (considering an optically thick reflecting layer this is equivalent to near unity absorption) can be achieved in the vicinity of a specific frequency range.[18–28] In one of the pioneering studies, Aydin *et al.*[29] demonstrated absorption above 0.71 in a range of 400 nm–700 nm, utilizing a symmetrical arrangement of a crossed trapezoid array in an MIM cavity configuration where the spacer layer thickness was much smaller than the operation wavelengths. Thereupon, this configuration was employed in several studies to obtain ultrabroadband light absorption with wider and stronger characteristics. Top metal layer patterns and dielectric spacer thickness were found to be crucial factors to achieve this ultrabroadband response. Nanopatches,[30–34] nanodiscs,[35–37] nanorings,[38] and other shapes[39] are examples of the employed geometries for top layer designs. In most of these designs, nanoresonant units with different shapes/dimensions are tuned in a way that the superposition of different resonances, arising from each unit, leads to an overall broadband absorber. However, all of the above designs have nanopattern configurations as their top metal layer, which are fabricated using the electron beam lithography (EBL) technique. Therefore, they have complex fabrication routes and they are not large scale compatible designs. In a recent study, it was theoretically and experimentally demonstrated that the use of planar unpatterned metal–insulator (MI) pairs can provide an ultra-broadband light absorption where the absorption bandwidth can extend to longer wavelengths by adding up the number of pairs.[40] After the study, a wide variety of MI combinations including W–Al_2O_3,[41] Cr–SiO_2,[42] Ag–Si,[43] and Ni–SiO_2 [44] were later utilized to improve the absorption capability of this architecture. A substantial enhancement in the light absorption capacity of these MI multilayer designs was achieved by the introduction of tapered configuration. This tapered scaffold provides a gradual impedance matching from air to the underlying multilayer absorber and consequently a larger absorption bandwidth can be achieved compared to the bare structure.[45–51] However, this improvement is achieved at the expense of adding complexity in the fabrication route of the design where the nanosized tapered etching of several periods of a MI multilayer requires multiple deposition and lithography processes.

Besides all of these studies that are mainly focused on the design architecture, there are very limited studies devoted to the study of designing the scaffold. As mentioned earlier, the main strategy in absorber designs is to superpose multiple resonances in a way that the overall response becomes broad. Some of the previous studies have achieved this characteristic by using different sized nanopatches. These multiple resonance characteristics can also be obtained utilizing elongated geometries such as nanowires or nanorods in which the excitation of multiple longitudinal surface plasmon modes can ensure an overall broad and strong light absorption. However, to date, there have been a few studies employing metal nanowires to realize perfect broadband light absorption.[52–55] This is mainly due to the fabrication complexity of these designs. Most of the methods for metallic nanowire fabrication are chemical-based processes in which synthesized nanowires/nanorods (that are dispersed inside a solution) are dropcast to another substrate.[52–54,56,57] Therefore, instead of free standing nanowires that are essential for light trapping, a planar-like configuration will be achieved in which nanowires are horizontally accumulated on each other and consequently longitudinal resonance modes cannot be efficiently excited throughout the design. Moreover, most of these chemically synthesized structures have a small aspect ratio which bounds their absorption edge to shorter wavelengths. A recent paper proposed an elegant design based on adiabatic nanofocusing of self-aggregated metallic nanowire bundle arrays to obtain ultra-broadband perfect absorption for steam generation applications.[58] However, this work also has multiple fabrication steps and to achieve absorption above 0.9, three layers should be stacked on each other, thereby making the overall design bulky. An alternative approach to obtain high aspect ratio nanowires is to coat metals on chemically synthesized dielectric nanowires. However, a full metal coverage on the nanowire surface is not possible using physical vapor deposition techniques (such as thermal evaporation and sputtering) due to the shadowing effect. This problem is even more detrimental in the case of randomly oriented dense dielectric nanowires that are the typical morphology of the chemical growth methods such as hydrothermal synthesis.

In the present paper, we propose a facial, large scale compatible, and lithography free design configuration to obtain perfect ultrabroadband light absorption. The architecture is made of hydrothermally grown TiO_2 nanowires uniformly coated with an ultrathin Pt metal layer deposited using an atomic layer deposition (ALD) tool. The synthesized nanowire design has a random orientation and high packing density which makes it an excellent scaffold for light trapping. Therefore, multiple reflections and transmissions from the Pt shell layer will provide perfect absorption throughout the whole visible (Vis) and near infrared (NIR) parts of the spectrum with an average amount of above 0.97. Our numerical simulation proves that these nanowires are able to support multiple longitudinal LSP modes in which the spectral position of these modes can be shifted to longer wavelengths by increasing the wire length. Moreover, due to the small thickness of the Pt coating, the structure acts as a bifacial absorber capable of providing perfect absorption for both front and rear illumination. Besides all of these characteristics, due to the random tilted orientation of nanowires, they can retain their absorption above 0.8 upon oblique angle excitation throughout their whole operation bandwidth. The use of hydrothermally grown TiO_2 nanowires, which is a chemical-based approach, makes the scaffold easy to be scaled up. Moreover, although coating the Pt layer with ALD is a slow process, it uses gaseous precursors to deposit the layer which makes it an excellent option to coat large areas with a high level of uniformity. It

should be noted that taking the excellent trapping capability of the nanowire structure into consideration, an ultrathin layer is enough to absorb the entire incoming light. Therefore, the proposed methodology opens up a new door for future photovoltaic technologies in which an ultrathin absorbing material coated on a suitable trapping scaffold can provide perfect ultrabroadband light absorption.

Results and discussion

Fig. 1 shows a schematic illustration of fabrication steps of the Pt coated TiO_2 nanowires. TiO_2 nanowires are first grown on an FTO coated glass substrate through a hydrothermal process as explained in the Experimental section and in our previous studies.[59–61] It should be noted that the hydrothermal process is a chemical-based method where the morphology of nanowires (length, diameter and density) can be controlled by tuning the growth conditions such as growth temperature, growth duration, seed layer morphology, and reactant concentration.[62–66] In the case of growth temperature and duration, the length and diameter of the nanowires are coupled to each other and the increase in one of them would lead to the increase in the dimension of the other one. A more precise control on the diameter of nanowires can be achieved by tuning the seed layer crystallinity.[62,65] The diameter of the grown nanowires is defined by the grain size of the seed layer in which smaller grain boundaries lead to smaller nanowires. It has been demonstrated that thinner seed layers have smaller grain boundaries and consequently they provide nanowires with smaller diameter and higher density. Another factor that can provide a better control on the lateral growth of nanowires is the initial reactant concentration.[63] As shown in Fig. 1a, the grown nanowires are densely packed and present random

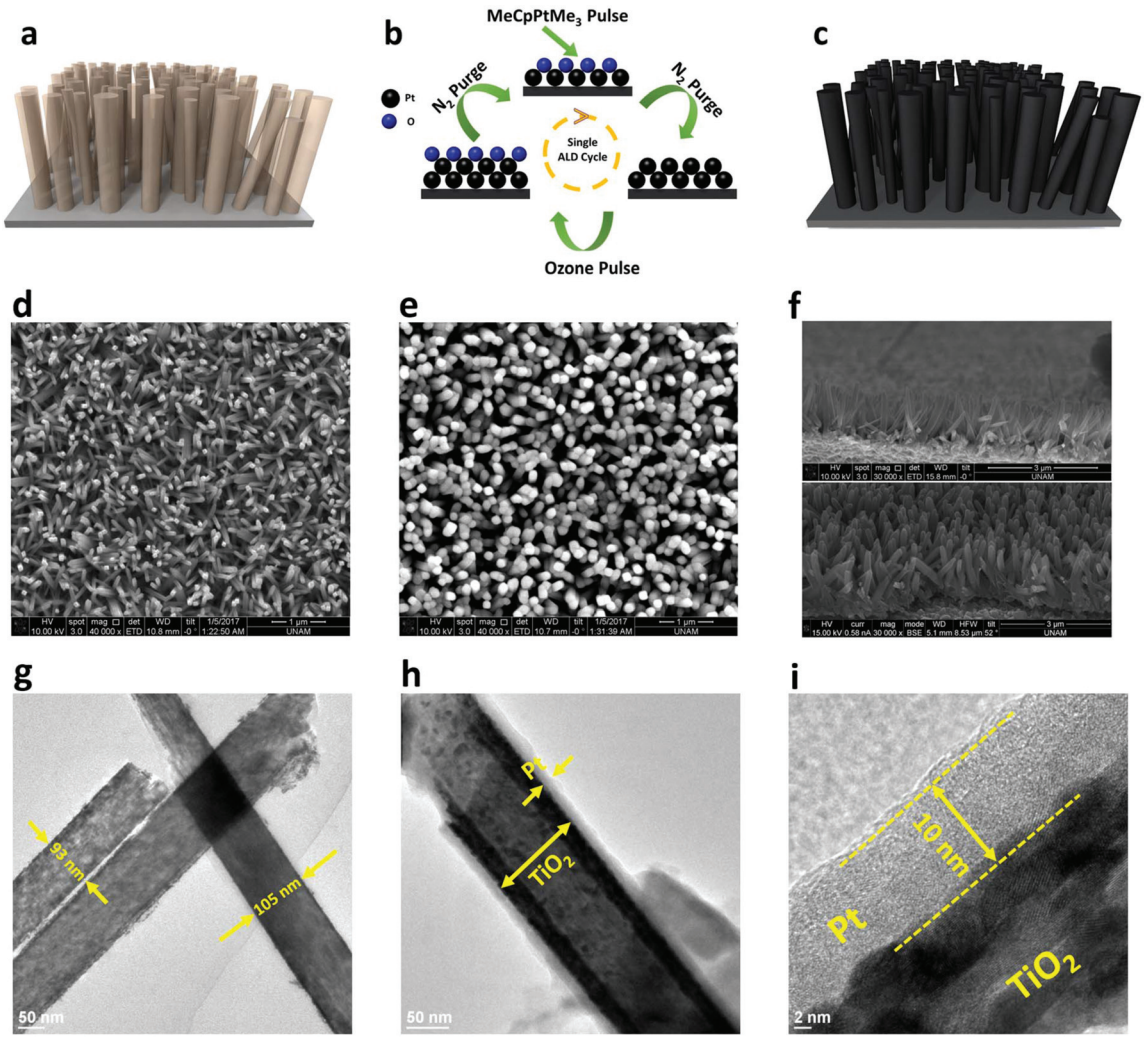

Fig. 1 Schematic illustration of the proposed (a) bare TiO_2 nanowire, (b) the ALD process to deposit the Pt shell, and (c) the resulting Pt-TiO_2 core–shell. Top SEM view of (d) bare and (e) Pt coated nanowires and (f) their cross-sectional image. A TEM image of (g) the bare TiO_2 nanowire and (h) the Pt coated core–shell structure, and (i) a high resolution TEM image showing the formation of a 10 nm Pt shell layer wrapping around the nanowire.

orientations. Afterward, these nanowires are placed in an atomic layer deposition (ALD) chamber and the Pt coating is carried out to our desired thickness. The unique properties of ALD have been exploited to form an ultrathin shell layer. ALD is built on self-limiting sequential surface reactions from at least two gas-phase molecular precursors and this technique offers pinhole-free ultrathin films with angstrom-scale thickness control. For this aim, ozone is utilized as an oxygen precursor and $MeCpPtMe_3$ solution for Pt metal atoms and, consequently, a Pt metal layer is uniformly coated on the surface of nanowires, as shown in Fig. 1b and c. The details of the experimental part have been provided in the ESI.† To structurally characterize the sample, a scanning electron microscope (SEM) and a transmission electron microscope (TEM) have been employed to investigate the morphology of layers and the dimensions of the nanowires. The SEM images shown in Fig. 1d and e reveal top views of the bare TiO_2 nanowire array and those coated with the Pt shell layer, respectively. On comparing these two images, one can conclude that the morphology of nanowires has not been altered upon deposition with a Pt layer that is expected taking the ALD process mechanism into consideration in which an ultrathin Pt layer is coated around a nanowire surface and the overall design shape that remains cylindrical. On the other side, the random orientation of nanowires can be easily distinguished in the cross sectional SEM view (Fig. 1f). Based on this image, nanowires have a wide length distribution ranging from 1000 nm to 1500 nm. The TEM image of the bare nanowire also shows that nanowires have an average diameter of 100 nm (Fig. 1g). The uniform formation of a thin Pt shell around titania nanowires has also been confirmed in Fig. 1h where this layer has a thickness of about 10 nm wrapped around the TiO_2 nanowire (as shown in a high resolution TEM image of Fig. 1i). It should be mentioned that the formation of the Pt layer is based on the nucleation of reactive sites. Therefore, in the first couple of nanometers (<10 nm), the morphology of the Pt shell is a nanoisland rather than a continuous layer (as shown in Fig. S1 (ESI†)). As the deposition continues, these nanoislands grow and finally a continuous layer is formed. This provides us a bottom up approach to control the resulting metal layer morphology.

To optically characterize our structure, in the first step, we need to know about the matching characteristics of Pt and compare it with other noble metals such as Au and Ag. For this aim, the effective permittivity of the Pt coated TiO_2 nanowire is predicted by the Maxwell–Garnett mixing rule for a mixture comprised of infinite-in-length circular cylinders that are a good approximation for our case where an aspect ratio of ~10 is recorded for the synthesized nanowires. Based on this theory, the effective permittivity of the core–shell nanowire (shown in Fig. 2a) can be calculated using the following formula:[67]

$$\varepsilon_{\text{eff}} = \varepsilon_s \frac{\varepsilon_c + \varepsilon_s + f(\varepsilon_c - \varepsilon_s)}{\varepsilon_c + \varepsilon_s - f(\varepsilon_c - \varepsilon_s)} \quad (1)$$

where ε_c is the permittivity of the core material (which is TiO_2) and ε_s represents the permittivity of the shell material which is the metal coating. The variable f also represents the area ratio between inner and outer cylinders which is defined by $f = (r_{in}/r_{out})^2$. From the predicted effective permittivity values, we calculate the refractive index (n) and extinction coefficient (k) where the reflectivity of the core–shell design is estimated using the following formula:

$$R = \left(\frac{n + ik - 1}{n + ik + 1}\right)^2 \quad (2)$$

Fig. 2b shows the reflectivity spectra calculated for 4 different metals of Au, Ag, Pt, and Cr. As can be seen from this panel, although all the metals represent good matching below 800 nm, this matching is lost in a longer wavelength for Au and Ag where a reflection near unity is recorded for these metals. However, both Pt and Cr maintain their matching well up to 2 μm which shows the absorption capacity of these metals in the proposed core–shell configuration. Therefore, Pt which we have used in our design has proper matching to obtain an ultrabroadband absorption response. Moreover, to understand the impact of the shell Pt layer on the reflectivity of the design, we swept the Pt layer thickness (d) from 5 nm to 25 nm. As shown in Fig. 2c, moving toward thicker layers, the matching condition of the core–shell design is lost in longer

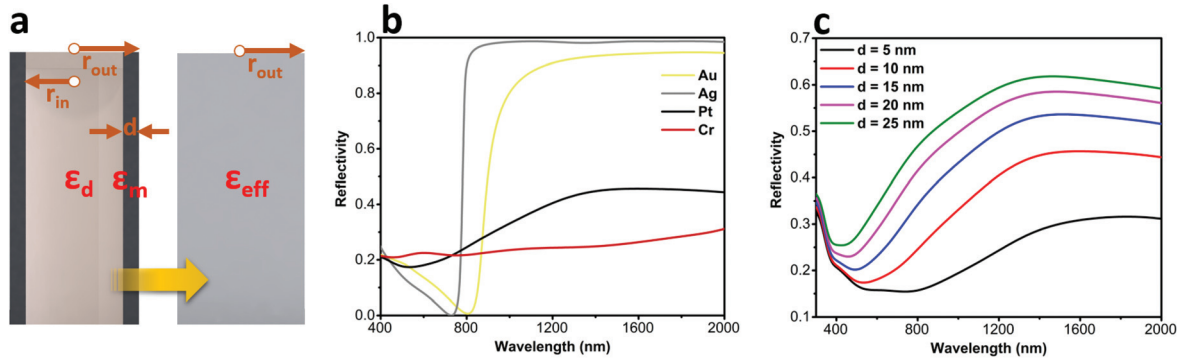

Fig. 2 (a) The proposed model for finding the effective permittivity of the core–shell design, and reflectivity spectra of (b) different metal types and (c) different Pt layer thicknesses.

wavelengths. However, on the other hand, it should be mentioned that although the thinner shell layer leads to less reflection from the design, the absorption capacity of the design will also be reduced due to its thickness. In addition, as mentioned in the previous section, the formation of a Pt continuous film is possible if the layer thickness reaches about 10 nm. Therefore, we fix the Pt layer thickness as d = 10 nm. As explained earlier, a one dimensional (1D) metallic nanostructure, where the structure is elongated in one dimension, can support multiple longitudinal resonant modes with transverse confinement along the nanowire surface. These supported modes, which are mainly longitudinal propagating and localized surface plasmon polaritons (SPPs) as well as transverse modes, are superposed and consequently an overall broad absorption response can be achieved. The longitudinal plasmon modes are essentially standing waves which can be explained by 1D damped Fabry–Perot cavity models. In other words, a nanowire can be considered as a monopole antenna where the resonant plasmon modes can be approximated by $m(\lambda_{sp}/2) \cong L$, where m is a positive integer number, L is the length of the nanowire and λ_{sp} is the surface plasmon polariton wavelength. Therefore, the multiple standing waves resonate at the wavelengths of $2L$, L, $2L/3$, ..., $2L/m$ in which the longer nanowire can provide a broader absorption bandwidth. To gain a better understanding of the nature of these modes, we performed numerical calculations employing a commercial finite-difference time-domain (FDTD) software package (Lumerical FDTD Solutions).[68] In the numerical simulations, the propagation direction of incident light is chosen to be perpendicular to the x–y plane. Periodic boundary conditions are also employed in the x and y directions, while boundaries in the z direction are adopted as a perfectly matched layer (PML). The unit cell periodicity P is chosen to be 200 nm and the Pt layer thickness is fixed at 10 nm. A broadband plane wave with polarization of the electric field along the x axis is utilized to stimulate the unit cell and reflected (R) and transmitted (T) lights are calculated by two monitors on two sides of the multilayer stack. Therefore, absorption (A) is calculated by using the equation $A = 1 - R - T$. In the initial step, the impact of the nanowire radius r is studied to understand the impact of this geometry under resonance conditions of the design. It should be mentioned that the length of the nanowire L is fixed at 1000 nm for this set of sweep. As can be clearly seen from Fig. 3a, several local maxima show the position of different resonant modes for different radius values where the longer resonances belong to the first resonant plasmon modes. For radii values r < 60 nm, these resonances are clear but when we move toward larger radii these peaks start to disappear and the overall absorption values decline. In fact, in large radius nanowires, the high filling factor makes the design to act like a planar reflecting layer. A more representative picture can be obtained by looking at the contour plot of the absorption values as a function of the wavelength and radius of the nanowire. As shown in Fig. 3b, there is only a slight shift in the position of absorption peaks, which is expected considering the fact that these resonances are longitudinal modes defined by the length of the nanowire. Moreover, lower order modes have wider spectral broadening (compared to higher order plasmon modes) that is the characteristics of standing waves. Another parameter that affects the overall light absorption capacity of the design is the length of the nanowires. Therefore, in the next step, we per-

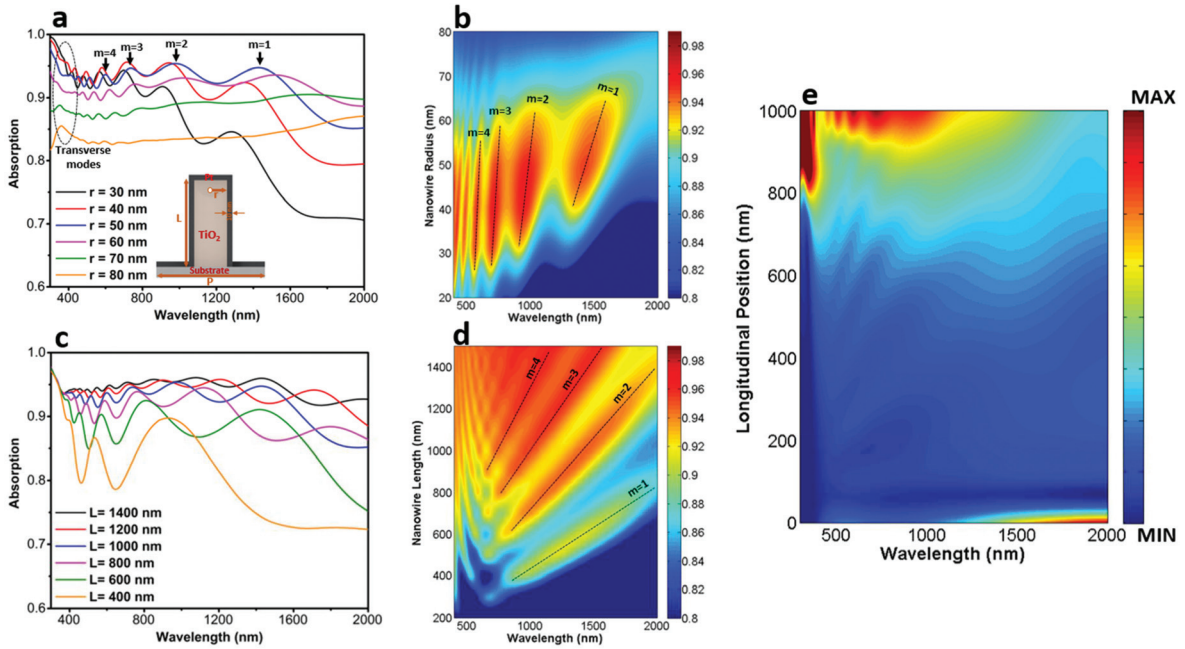

Fig. 3 The absorption spectra and contour plot of different nanowire (a, b) radii and (c, d) lengths. (e) The absorption profile through the nanowire length as a function of the excitation wavelength.

formed a sweep on the length of the nanowires. The same as radius dependence, the spectra show multiple resonances proving the formation of different orders of plasmon modes, as shown in Fig. 3c. However, the position of absorption peaks gains larger shifts compared to the previous case that is expected considering the fact that these modes are mainly longitudinal modes. Fig. 3d shows the dependence of the peak position on the lengths of the nanowires. As can be clearly deduced from this figure, first order modes have lower amplitudes compared to the larger ones. As the order of modes is increased, not only a peak amount becomes larger but also the coupling between modes becomes stronger and the overall absorption values approach unity. Fig. 3e illustrates the absorption profile of the nanowire as its longitudinal position. According to all of these results, one can conclude that a random design, where different sized nanowires (both radius and length) are brought together, can provide a near unity flat absorption response due to the superposition of adjacent resonant modes. Based on this plot, the absorption in the shorter wavelengths is concentrated in the top edge of the nanowire. As we go to longer wavelength values, light diffuses deeper into the nanowire array and consequently the absorption confinement is shifted into the bottom edge of the wire.

To gain a better insight into the formation of the longitudinal modes across the nanowire, the field profiles of different wavelengths of λ = 500 nm, 1000 nm, and 2000 nm are plotted in Fig. 4a–i. Fig. 4a–c clearly show the formation of an electric field (E field) standing wave along the nanowire length where the number of peaks and nodes are increased when the incident light wavelength becomes shorter. In other words, the resonance at 2000 nm is due to the fundamental mode, while the one at 500 nm represents higher order modes. The same pattern can also be found for a magnetic field (H field), as shown in Fig. 4d–f. Both E field and H field distributions reveal that we have a large absorption cross-section in the space between nanowires where the position dependence of these power distributions alters with the order of modes. Moreover, the E field distributions of the design for these three different wavelengths are plotted in Fig. 4g–i. As these panels clearly illustrate, wavefronts of the plane wave have not been disturbed upon impinging the nanowire array design. This proves excellent matching between air and the nanowire structure where an almost zero reflection is recorded on the surface of the nanowire array. In other words, upon the excitation of the structure with a plane wave, the light diffuses into the design and it gets trapped there where the diffusion length of the light increases when we move to longer wavelengths; this is in line with our previous results as shown in Fig. 3e.

Another prominent factor affecting the absorption spectra of the nanowires is their orientation. Fig. 5 shows the absorption spectra of vertically standing and tilted nanowires. The

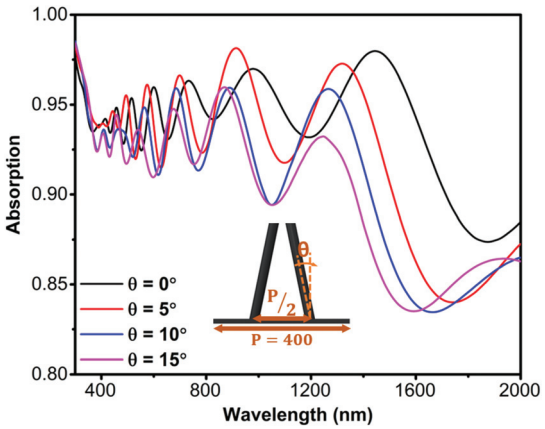

Fig. 5 The absorption spectra of vertically and tilted standing nanowires.

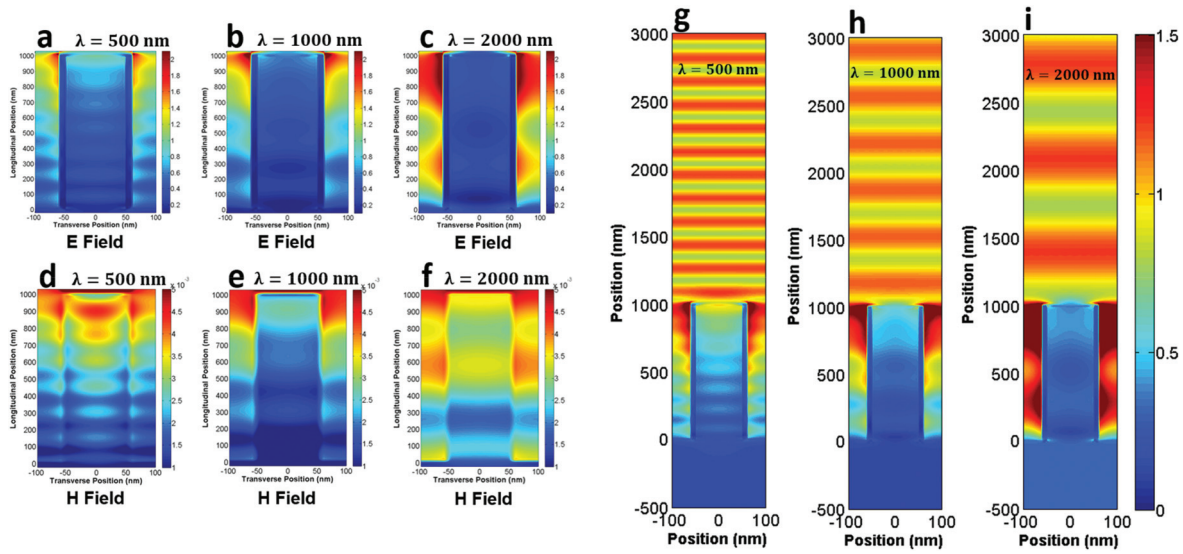

Fig. 4 (a, b, c) Electric field, (d, e, f) magnetic field and (g, h, i) mode profiles of different three incidence wavelengths of 500 nm, 1000 nm, and 2000 nm.

unit cell employed in our simulations for this case is shown in the inset. This panel shows that a slight tilt in the orientation of nanowires makes a blue shift in the resonance frequency. Looking at this graph, similar to the radius and length of nanowires, one can understand that a randomly oriented nanowire array (as in our case) can have a response that is the superposition of these resonances and, therefore, a flat near unity absorption can be obtained for this architecture. Essentially, the randomly oriented nanowires (rather than vertically aligned ones) are an excellent scaffold to trap the light. Thus, all the numerical findings prove that our synthesized nanowires should form an excellent absorber with a strong light absorption capacity and ultra-broadband response. To evaluate our findings, we have fabricated the design and the optical characterization is conducted on the sample to scrutinize the absorption capacity of the nanowire design. As explained in the previous parts and schematically illustrated in Fig. 6a, the densely packed randomly oriented Pt coated TiO_2 nanowires are excellent light harvesting architectures. The light impinging on this design will be entirely trapped inside the design and absorption near unity will be recorded for this configuration. This can be easily recognized from the comparison between bare TiO_2 nanowires and Pt coated ones, as shown in Fig. 6b. For a black background, the Pt coated nanowire sample can be barely distinguished from the underlying color estimating a high absorption amount in the visible range. In addition to this, the bare nanowire structure has a white non-transparent color that proves its high trapping capacity. Fig. 6c shows the absorption spectra of the sample measured in the integrated sphere setup. The transmission and reflection results have been analysed and the absorption values have been calculated from these data. As can be implied from this graph, absorption above 0.97 is measured throughout an ultra-broadband spectrum spanning from 370 nm to 1100 nm. The measurement has been limited to this range due to equipment limitations. To understand the response of the sample in the longer wavelength values, we have applied oblique angle measurements using ellipsometry equipment for both transverse magnetic (TM) and transverse electric (TE) polarizations. It should be mentioned that due to the existence of nanowires in the design, we should have high scattering from designs. However, our design is a highly absorptive trapping design where light is trapped inside the nanostructures and after several scattering, it gets absorbed before it leaves the structure. This can be confirmed by comparing the absorption spectra obtained from the integrated sphere setup (Fig. 6c) and ellipsometry results (Fig. 6d and e) where a fair matching is recorded for these two sets of data. As Fig. 6d and e obviously illustrates, the structure maintains its absorption response high even at higher incidence angles. For both TM and TE polarizations, the absorption values remains above 0.9 for angles as wide as 60°, and for an angle of θ = 70° the response is still above 0.8 throughout the whole studied spectrum. These results are expected considering the high aspect ratio of nanowires and their random orientation that make the design functional through wide incidence angles.

Another unique property of this design configuration is its bifacial absorption capability. Essentially, in most of the plasmonic designs, a back reflecting layer is required to obtain high broadband absorption. The back reflector coating sends

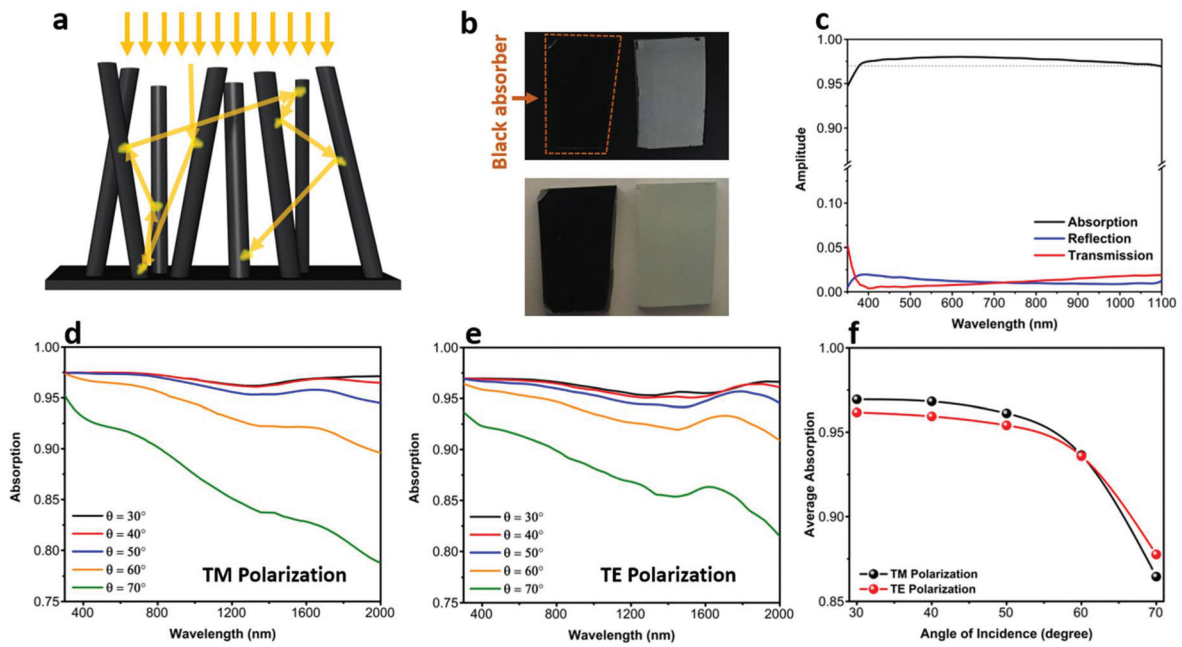

Fig. 6 (a) Trapping capability of a randomly oriented nanowire design, (b) the image of the sample proving its black color, (c) normal incident light absorption spectra of the black sample and its oblique angle response to (d) TM and (e) TE polarizations, and (f) average light absorption values as a function of the incident light angles.

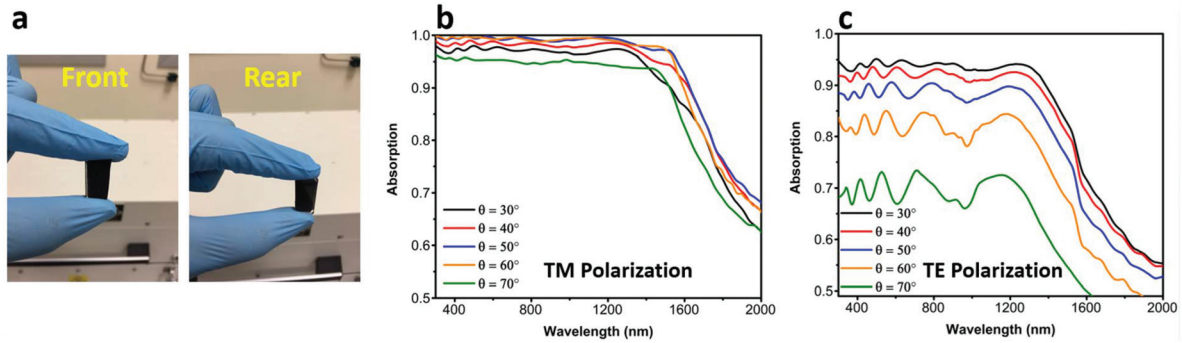

Fig. 7 (a) The front and rear appearance of the nanowire sample and its angular response to (b) TM and (c) TE polarized excitation light.

the light back into the cavity and absorption near unity is achieved across an ultra-broadband frequency range. The existence of the back mirror layer makes the design highly reflective in one direction. However, in our design, the use of an ultrathin metal layer, where it is partially coated on the substrate (in the places that we do not have the nanowire), makes the device responsive even under rear illumination. Fig. 7a shows the black appearance of the nanowire design under both front and rear illumination. To be able to characterize its longer wavelengths, similar to the previous part, we have made oblique angle absorption measurements for both TM and TE polarizations, as shown in Fig. 7b and c. Based on these results, for TM polarization, the absorption remains above 0.9 up to 1600 nm in which an abrupt reduction is recorded in the longer wavelengths. However, TE polarized light loses its absorption strength in a very sharp way in which an average absorption of 0.9 for $\theta = 30°$ declines to an amount as small as 0.7 for $\theta = 70°$ light incidence.

Conclusions

In summary, in this study, we design, fabricate, and characterize an ultrabroadband bifacial wide angle absorber in Vis and NIR frequency regimes. Our absorber architecture is made of Pt coated TiO_2 nanowires where these nanowires have a high packing density and random orientation which make them an excellent light trapping candidate. Our numerical findings demonstrate that the absorption edge of the structure can be extended toward longer wavelengths by increasing the nanowire length. This paper reveals the importance of the scaffold where by taking unique advantages of the ALD method, together with the excellent light trapping of chemically synthesized nanowires, a large scale compatible absorber design can be realized where a near perfect absorption is obtained while using fewer materials.

Conflicts of interest

There are no conflicts to declare.

Acknowledgements

This work is supported by the projects DPT-HAMIT and TUBITAK under Project No. 113E331 and 109E301. One of the authors (E. O.) also acknowledges partial support from the Turkish Academy of Sciences.

Notes and references

1 P. Mandal, *Plasmonics*, 2016, **11**, 223–229.
2 S. W. Luo, J. Zhao, D. L. Zuo and X. B. Wang, *Opt. Express*, 2016, **24**, 9288–9294.
3 Z. Yong, S. Zhang, C. Gong and S. He, *Sci. Rep.*, 2016, **6**, 24063.
4 A. Tittl, P. Mai, R. Taubert, D. Dregely, N. Liu and H. Giessen, *Nano Lett.*, 2011, **11**, 4366–4369.
5 K. Chen, R. Adato and H. Altug, *ACS Nano*, 2012, **6**, 7998–8006.
6 Y. Li, L. Su, C. Shou, C. Yu, J. Deng and Y. Fang, *Sci. Rep.*, 2013, **3**, 2865.
7 E. Rephaeli and S. Fan, *Opt. Express*, 2009, **17**, 1421–1424.
8 C. Wu, B. Neuner III, J. John, A. Milder, B. Zollars, S. Savoy and G. Shvets, *J. Opt.*, 2012, **14**, 24005.
9 W. Li and J. Valentine, *Nano Lett.*, 2014, **14**, 3510–3514.
10 Z. Yang, L. Ci, J. A. Bur, S. Lin and P. M. Ajayan, *Nano Lett.*, 2008, **8**, 446–451.
11 N. I. Landy, S. Sajuyigbe, J. J. Mock, D. R. Smith and W. J. Padilla, *Phys. Rev. Lett.*, 2008, **100**, 207402.
12 W. Chang, J. Won, L. S. Slaughter and S. Link, *Proc. Natl. Acad. Sci. U. S. A.*, 2010, **107**, 2781–2786.
13 Y. Avitzour, Y. A. Urzhumov and G. Shvets, *Phys. Rev. B: Condens. Matter*, 2009, **79**, 1–5.
14 H. Tao, C. M. Bingham, D. Pilon, K. Fan, A. C. Strikwerda, D. Shrekenhamer and W. J. Padilla, *J. Phys. D: Appl. Phys.*, 2010, **43**, 225102.
15 Q. Wen, Y. Xie, H. Zhang, Q. Yang and Y. Li, *Opt. Express*, 2009, **17**, 20256–20265.
16 N. Liu, M. Mesch, T. Weiss, M. Hentschel and H. Giessen, *Nano Lett.*, 2010, **10**, 2342–2348.

17 J. Hao, J. Wang, X. Liu, W. J. Padilla, L. Zhou and M. Qiu, *Appl. Phys. Lett.*, 2010, **96**, 251104.
18 M. Yan, *J. Opt.*, 2013, **15**, 25006.
19 K. Q. Le and J. Bai, *J. Opt. Soc. Am. B*, 2015, **32**, 595–599.
20 X. Chen, Y. Shi, F. Lou, Y. Chen, M. Yan, L. Wosinski and M. Qiu, *Opt. Express*, 2014, **22**, 549–551.
21 C. Koechlin, P. Bouchon, F. Pardo, J. Pelouard and R. Ha, *Opt. Express*, 2013, **21**, 4641–4647.
22 J. O. H. Endrickson and J. U. G. Uo, *J. Opt. Soc. Am. B*, 2015, **32**, 1686–1692.
23 Y. Chen, J. Dai, M. Yan and M. Qiu, *Opt. Express*, 2014, **22**, 4641–4647.
24 L. Lin and Y. Zheng, *Sci. Rep.*, 2015, **5**, 14788.
25 W. Wang, D. Zhao, Y. Chen, H. Gong, X. Chen, S. Dai, Y. Yang, Q. Li and M. Qiu, *Opt. Express*, 2014, **22**, 5416–5421.
26 X. Lu, R. Wan and T. Zhang, *Opt. Express*, 2015, **23**, 29842.
27 J. Yang, C. Sauvan, A. Jouanin, S. Collin, J.-L. Pelouard and P. Lalanne, *Opt. Express*, 2012, **20**, 16880.
28 S. Collin, G. Li, X. Chen, O. Li and C. Shao, *J. Phys. D: Appl. Phys.*, 2012, **45**, 205102.
29 K. Aydin, V. E. Ferry, R. M. Briggs and H. a. Atwater, *Nat. Commun.*, 2011, **2**, 517.
30 Q. Feng, M. Pu, C. Hu and X. Luo, *Opt. Lett.*, 2012, **37**, 2133–2135.
31 O. Communications, *Opt. Lett.*, 2017, **42**, 450–453.
32 Y. Zhang, L. Zhou, J.-Q. Li, Q.-J. Wang and C.-P. Huang, *Sci. Rep.*, 2015, **5**, 10119.
33 H. Wang and L. Wang, *Opt. Express*, 2013, **21**, 13311–13319.
34 W. E. G. Uo, Y. U. L. Iu and T. I. H. An, *Opt. Express*, 2016, **24**, 20586–20592.
35 F. Ding, J. Dai, Y. Chen, J. Zhu, Y. Jin and S. I. Bozhevolnyi, *Sci. Rep.*, 2016, **6**, 39445.
36 Y. Lu, W. Dong, Z. Chen, A. Pors, Z. Wang and S. I. Bozhevolnyi, *Sci. Rep.*, 2016, **6**, 30650.
37 M. G. Nielsen, A. Pors, O. Albrektsen and S. I. Bozhevolnyi, *Opt. Express*, 2012, **20**, 13311–13319.
38 D. Hu and H. Wang, *J. Nanophotonics*, 2016, **10**, 26021.
39 G. Tagliabue, H. Eghlidi and D. Poulikakos, *Nanoscale*, 2013, **5**, 9957–9962.
40 N. Mattiucci, M. J. Bloemer, N. Aközbek and G. D'Aguanno, *Sci. Rep.*, 2013, **3**, 3203.
41 M. Chirumamilla, A. S. Roberts, F. Ding, D. Wang, P. K. Kristensen, S. I. Bozhevolnyi and K. Pedersen, *Opt. Mater. Express*, 2016, **6**, 2704–2714.
42 H. Deng, Z. Li, L. Stan, D. Rosenmann and D. Czaplewski, *Opt. Lett.*, 2015, **40**, 2592–2595.
43 G. Kajtár, M. Kafesaki, E. N. Economou and C. M. Soukoulis, *J. Phys. D: Appl. Phys.*, 2016, **49**, 55104.
44 Y. K. Zhong, Y.-C. Lai, M.-H. Tu, B.-R. Chen, S. M. Fu, P. Yu and A. Lin, *Opt. Express*, 2016, **24**, A832.
45 Y. Cui, K. H. Fung, J. Xu, Y. Jin, S. He and N. X. Fang, *Nano Lett.*, 2012, **12**, 1443–1447.
46 F. Ding, Y. Jin, B. Li, H. Cheng, L. Mo and S. He, *Laser Photonics Rev.*, 2014, **8**, 946–953.
47 F. Ding, Y. Cui, X. Ge, Y. Jin and S. He, *Appl. Phys. Lett.*, 2012, **100**, 103506.
48 X. Yin, C. Long, J. Li, H. Zhu, L. Chen, J. Guan and X. Li, *Sci. Rep.*, 2015, **5**, 15367.
49 Q. Liang, W. Yu, W. Zhao, T. Wang, J. Zhao, H. Zhang and S. Tao, *Opt. Mater. Express*, 2013, **3**, 376–379.
50 C. Long, S. Yin, W. Wang, W. Li, J. Zhu and J. Guan, *Sci. Rep.*, 2016, **6**, 21431.
51 X. He, S. Yan, G. Lu, Q. Zhang, F. Wu and J. Jiang, *RSC Adv.*, 2015, **5**, 61955–61959.
52 V. A. Online, S. Kim, K. Imura, M. Lee, T. Narushima, H. Okamoto and D. H. Jeong, *Phys. Chem. Chem. Phys.*, 2013, **15**, 4146–4153.
53 H. Wei, A. Reyes-coronado, P. Nordlander, J. Aizpurua and H. Xu, *ACS Nano*, 2010, **4**, 2649–2654.
54 X. Chen, H. Gong, S. Dai, D. Zhao, Y. Yang, Q. Li and M. Qiu, *Opt. Lett.*, 2013, **38**, 2247–2249.
55 Y. Han, J. Huang, X. Liu, X. Zhang, J. Shi and C. Yan, *Opt. Express*, 2016, **24**, 9178–9186.
56 H. Jia, C. Fang, X. Zhu, Q. Ruan, Y. J. Wang and J. Wang, *Langmuir*, 2015, **31**, 7418–7426.
57 H. Chen, L. Shao, Q. Li and J. Wang, *Chem. Soc. Rev.*, 2013, **42**, 2679–2724.
58 K. Bae, G. Kang, S. K. Cho, W. Park, W. J. Padilla and K. Kim, *Nat. Commun.*, 2015, **6**, 1–9.
59 A. Ghobadi, T. G. Ulusoy, R. Garifullin, M. O. Guler and A. K. Okyay, *Sci. Rep.*, 2016, **6**, 30587.
60 A. Ghobadi, H. I. Yavuz, T. G. Ulusoy, K. C. Icli, M. Ozenbas and A. K. Okyay, *Electrochim. Acta*, 2015, **157**, 23–30.
61 T. G. Ulusoy, A. Ghobadi and A. K. Okyay, *J. Mater. Chem. A*, 2014, **2**, 16867–16876.
62 S. Nadzirah, U. Hashim and T. Adam, Fifth Int. Conf. Intell. Syst. Model. Simul., 2014, 6–9.
63 J. Su and L. Guo, *RSC Adv.*, 2015, **5**, 53012–53018.
64 B. Liu and E. S. Aydil, *J. Am. Chem. Soc.*, 2009, **131**, 3985–3990.
65 J. Song and S. Lim, *J. Phys. Chem. C*, 2007, **111**, 596–600.
66 I. S. Cho, Z. Chen, A. J. Forman, D. R. Kim, P. M. Rao, T. F. Jaramillo and X. Zheng, *Nano Lett.*, 2011, **11**, 4978–4984.
67 A. H. Panaretos, Y. A. Yuwen, D. H. Werner and T. S. Mayer, *Sci. Rep.*, 2015, **5**, 9813.
68 Lumerical Solut. Inc. http://www.lumerical.com/tcad-products/fdtd/.

